Fault-Tolerant Control of Nine-Phase Induction Motor With Sensorless Speed and Flux Estimation

Nithin S. Nair
Department of EEE
NIT Calicut
Calicut, Kerala, India
nithin232010@gmail.com

Priyanka C. P.
Department of EEE
NIT Calicut
Calicut, Kerala, India
Priyanka_p180050ee@nitc.ac.in

Jagadanand G.
Department of EEE
NIT Calicut
Calicut, Kerala, India
jagadanand@nitc.ac.in

2022 IEEE International Conference on Power Electronics, Drives and Energy Systems (PEDES) | 978-1-6654-5566-4/22/$31.00 ©2022 IEEE | DOI: 10.1109/PEDES56012.2022.10080087

***Abstract*—Design and application of fault-tolerant control (FTC) in multiphase drives are essential in safety-relevant applications such as electric vehicles, space vehicle drives, chemical industrial drives etc. A nine-phase motor endure to operate with rotating magnetic field (RMF) as long as no more than six phases are faulted. This paper proposes a fault-tolerant control for nine-phase induction motor drive, in which a single switch open-circuit fault is occurred in the nine-phase inverter feeding the motor. The proposed FTC reconfigures the current references to the motor controller in such a way to avoid the overheating in healthy phases due to stator copper losses. A sensorless field-oriented control is employed for the speed and torque control of motor drive. The proposed sensorless control scheme employs an Extended Kalman Filter (EKF) algorithm to estimate the rotor speed, rotor flux, and rotor field position without using any speed and flux sensors which make the system more reliable and less sensitive to motor parameter variations, disturbances, and speed encoder faults. Credibility of the proposed FTC is evaluated in MATLAB/SIMULINK platform.**

Keywords—Fault-tolerant control, Nine-phase inverter, Direct vector control, Nine-phase induction motor, Extended Kalman filter

NOMENCLATURE

n_p	Number of poles in machine
$v_a - v_i$	Motor terminal phase voltages
$i_a - i_i$	Motor phase currents
T_e	Torque developed in motor
ω_r	Rotor speed in electrical radian/second
ω_1	Fundamental angular frequency
ω_e, θ_e	Speed and position of rotor field
T_s	Sampling period
$\hat{I}$	Peak value of phase current in healthy case
φ	Electrical special angle
θ	Electrical phase angle
$i_{s\alpha}, i_{s\beta}$	Stator current components in stator reference frame
V_{dc}	DC bus voltage
$v_{s\alpha}, v_{s\beta}$	Stator voltage components in stationary reference frame
i_{ds}, i_{qs}	Stator current components in rotor flux reference frame
$\lambda_{r\alpha}, \lambda_{r\beta}$	Rotor flux components in stationary reference frame
T_r	Rotor time constant
σ	Leakage coefficient in machine
F_{max}	Maximum value of airgap mmf

I. INTRODUCTION

Multiphase motor drives are now becoming prominent among both academic community and industry as compared to three-phase counterpart due to their high power density, less torque ripple, fault-tolerant capability, reduced space harmonics, reduced motor phase currents without increasing the phase voltage, less filter requirements, higher degree of freedom to apply advanced control strategies, and moreover reliability. [1], [2]. The above said advantages make the multiphase drives a best option for safety-relevant low voltage, high power applications such as battery and hybrid electric vehicles, more-electric aircrafts, and ship propulsion [3], [4]. However, the control complexity of multiphase induction motor (IM) drive is high compared to three-phase drives, the developments and advancements in power electronics and digital signal processors enhance the multiphase IM drive in high performance industrial applications [4], [5].

The majority of fault in a multiphase IM drive emanates from power electronic converters. The early-stage fault detection and isolation is crucial in high performance drives in view of economy and safety. Following the fault isolation stage, appropriate fault-tolerant control is to be applied to prevent performance degradation of the motor drive system. In this paper, a fault-tolerant control (FTC) is developed for the nine-phase induction motor drive system in which single switch open-circuit (OC) fault is occurred in two-level, nine-phase inverter.

Cost, output performance such as voltage total harmonic distortion (THD), torque ripples, dynamic performance of the drive etc., are the main considerations for FTC. Fault-tolerant control proposed in this paper develops an optimum set of reference phase currents so that motor's stator copper losses are same both in pre- and post-fault conditions. The problem of designing the fault-tolerant control is to find an appropriate relationship between the stator currents of healthy phases so that the operation with undisturbed rotating magnetic field (RMF) is obtained. Out of different fault tolerant algorithms, method of symmetrical components is utilized in this paper. The Vector Space Decomposition (VSD) technique is used to control asymmetric phase currents during the fault conditions under rotor field-oriented synchronous frame. For a nine-phase drive, with VSD, the physical current components on stator reference frame are converted onto four sets of orthogonal subspaces: one torque-generating subspace and three harmonic subspaces.

In this paper, the nine-phase induction machine (IM) is modelled using multiple d-q spaces concept [3]- [6]. The fault-

978-1-6654-5566-4/22/$31.00 ©2022 IEEE

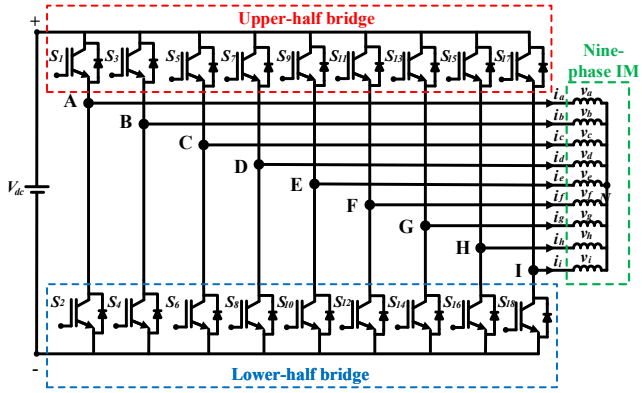

Fig. 1. Power circuit of two-level nine-phase inverter feeding induction motor

tolerant control solution is achieved with rotor field-oriented control (RFOC). The main drawback of field-oriented control is the field position error due to variations in parameters or uncertainties together with measurement noise [16]. Therefore, in order to improve the drive performance, Extended Kalman Filter (EKF) is employed for the estimation of motor angular speed and rotor flux orientation. The sensorless algorithm improves the system reliability in terms of rotor speed sensor faults. The effectiveness of proposed fault-tolerant control in the event of inverter OC fault and during various speed-torque operating conditions of the motor drive is studied using MATLAB/SIMULINK.

II. Fault Tolerant Control (FTC)

The main objectives of FTC are to minimize the torque pulsations and machine losses during the open-circuit (OC) fault in the multiphase inverter and/or motor. A two-level nine-phase inverter driving a nine-phase induction motor with single neutral point is considered in this paper, whose power circuit is given in Fig. 1. Single neutral point facilitates the utilization of all the remaining healthy phases for post-fault operation of the drive [8]- [10]. The phase grouping and current orientation during pre-fault operation is shown in Fig. 2. The phase displacement between the phases is 40^0. The fault detection and localisation are the first stage of implementing the fault-tolerant operation which is performed using machine phase voltages discussed in [11]. For the two-level inverters, the faulty phase is to be removed when any power switch fails in that phase leg before applying the FTC.

If one phase of the multiphase drive is open circuit, the remaining healthy phase currents are to be reconstituted to generate an undisturbed rotating magnetic field (RMF) in the machine. The FTC criteria used in this paper is minimum stator copper loss under open-circuit fault. Out of several FTC algorithms, method of symmetrical components is employed in this work to modify the stator current references to yield the RMF and guarantee the stator copper loss below the rated value in post-fault conditions [8]- [12]. The orientation of motor currents to generate RMF during post-fault operation is shown in Fig. 3. As the main objective of FTC is to maintain stator copper loss within the rated value, the current magnitude may differ from the nominal value during post-fault operation as shown in Fig. 3.

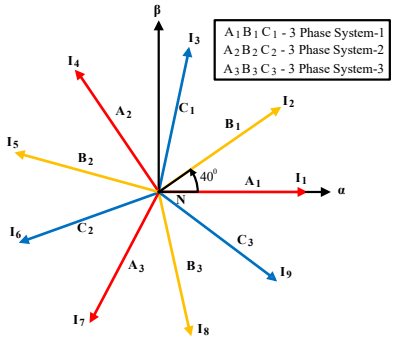

Fig. 2. Phase grouping and motor phase current orientation during pre-fault operation

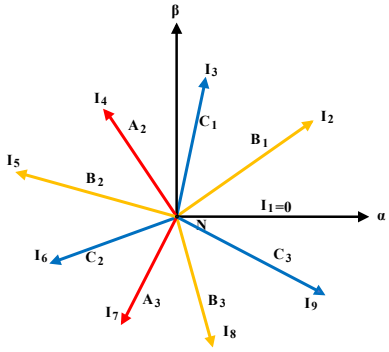

Fig. 3. Motor phase current orientation during post-fault operation

The block diagram of FTC using RFOC drive is shown in Fig. 4. When O.C. fault occurs, current references generated by the control system will contain double frequency components. So, two pairs of PI controllers, one operated in the synchronous reference frame rotating at a speed of ω_1 and the other in the synchronous reference frame rotating at a speed of $-\omega_1$ are used to control the non-sinusoidal currents in the harmonic subspaces [5], [6]. The reference currents are generated based on the torque and speed demand. These reference currents are modified by the FTC as shown in Fig. 4. The speed and rotor field position are estimated by the EKF algorithm with stator voltages and currents in stationary reference frame as the inputs [13]- [15]. The estimated states are rotor speed, rotor flux, and rotor field position. The application of the EKF to the discrete state-space model of the induction machine, will consider the presence of state noise and measurement noise in the drive [8].

The stator windings of nine-phase induction motor are treated as three-star windings with a space displacement of 40 deg. with each other and during the balanced and healthy conditions, the RMF is given by:

$$MMF_{normal} = 9/2 * F_{max}\, sin(\varphi - \theta) \qquad (1)$$

When an O.C. fault occurs in any of the phase legs, the system will produce negative sequence MMF and zero sequence current which must be eliminated and maintain the positive sequence MMF same as pre-fault value.

Let phase-1 is open-circuited (phase system-1) and $i_1 = 0$. MMF produced by phase system-1 is given by (2).

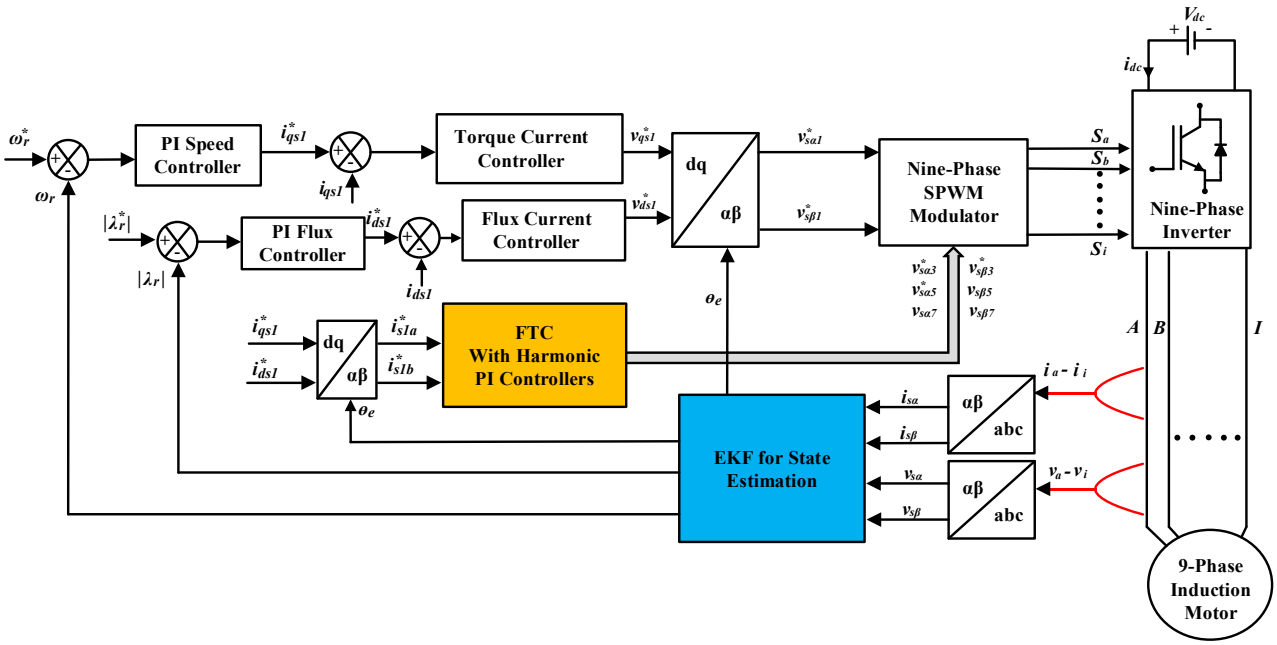

Fig. 4. Block schematic of RFOC with FTC and EKF-based state estimation

$$MMF_1 = F_{max}[i_1 * sin(\varphi) + i_4 * sin(\varphi + 120^0) + i_7 * sin(\varphi + 240^0)] = F_{max}\, sin(\varphi - \theta) - 0.5 * F_{max}\, sin(\varphi + \theta) \quad (2)$$

The zero-sequence current is given by:

$$I_{0(1)} = -\frac{1}{3}\hat{I}\, cos(\theta) \quad (3)$$

The positive sequence MMF and negative sequence MMF of healthy systems are given by (4) and (5) respectively.

$$MMF_{2,\,3(+)} = \frac{7}{4}F_{max}\, sin(\varphi - \theta) \quad (4)$$

$$MMF_{2,3(-)} = \frac{1}{4}F_{max}\, sin(\varphi + \theta) \quad (5)$$

The zero-sequence current of healthy systems is given by:

$$I_{0(2,3)} = \frac{1}{6}\hat{I}\, cos(\theta) \quad (6)$$

Now we can find the symmetrical currents of healthy systems using MMF expression. Adding the sequence components will result in reference phase currents in physical variables. Transform these current references into 4 orthogonal subspaces using VSD approach. The amplitude of positive and negative sequence currents of healthy systems are given by:

$$I_m^+ = \frac{2}{3} * \frac{7}{4} = 1.167 * \hat{I}\, pu \text{ and } I_m^- = \frac{2}{3} * \frac{1}{4} = 0.167 * \hat{I}\, pu \quad (7)$$

III. Extended Kalman Filter (EKF) for Rotor Field-Oriented Control (RFOC)

The effectiveness of FTC in nine-phase IM drive is evaluated using RFOC with synchronous reference current control. The accurate values of rotor flux magnitude, rotor field position, and rotor speed are estimated using EKF whose stochastic characteristics are well suited to uncertainties and parameter variations within the IM model [17]. It will perform the online estimation of rotor field position and speed under wide range of speed-torque profile while considering the IM model errors and measurement errors/noises in the IM drive system.

The fifth-order discrete state space model of nine-phase IM is considered for state estimation using EKF algorithm with rotor flux, rotor speed, and stator current as state variables.

$$X_{e(k+1)} = f\left(X_{e(k)}, U_{(k)}\right) + W_{(k)} = A_d X_{e(k)} + B_d U_{(k)} + W_{(k)} \quad (8)$$

$$Y_{(k)} = h\left(X_{e(k)}\right) + V_{(k)} = C_d X_{e(k)} + V_{(k)} \quad (9)$$

$$X_{e(k)} = \left[i_{s\alpha(k)}\; i_{s\beta(k)}\; \lambda_{r\alpha(k)}\; \lambda_{r\beta(k)}\;\; \omega_{r(k)}\right]^T \quad (10)$$

$$U_{(k)} = \left[v_{s\alpha(k)}\; v_{s\beta(k)}\right]^T;\; Y_{(k)} = \left[i_{s\alpha(k)}\; i_{s\beta(k)}\right]^T \quad (11)$$

Here,

$$A_d = \begin{bmatrix} a_1 & 0 & a_2 & a_3 * \omega_r & 0 \\ 0 & a_1 & -a_3 * \omega_r & a_2 & 0 \\ a_4 & 0 & a_5 & -T_s * \omega_r & 0 \\ 0 & a_4 & T_s * \omega_r & a_5 & 0 \\ -a_7 & a_8 & 0 & 0 & a_6 \end{bmatrix}$$

$$B_d = \begin{bmatrix} b_1 & 0 & 0 & 0 & 0 \\ 0 & b_1 & 0 & 0 & 0 \end{bmatrix}^T ; C_d = \begin{bmatrix} 1 & 0 & 0 & 0 & 0 \\ 0 & 1 & 0 & 0 & 0 \end{bmatrix}$$

$$a_1 = 1 - ((R_s * T_s)/(\sigma * L_s) + ((1-\sigma) * T_s)/(\sigma * T_r))$$

$$a_2 = T_s * ((1-\sigma)/(\sigma * T_r * L_m));$$

$$a_3 = T_s * ((1-\sigma)/(\sigma * L_m)); a_4 = T_s * L_m/T_r$$

$$a_5 = 1 - (T_s/T_r); a_6 = 1 - (b * T_s/J)$$

$$a_7 = (9 * n_p * n_p * L_m * T_s * T_s * \lambda_{r\beta})/(8 * J * L_r)$$

$$a_8 = (9 * n_p * n_p * L_m * T_s * T_s * \lambda_{r\alpha})/(8 * J * L_r)$$

$$b_1 = T_s/(\sigma * L_s); \sigma = 1 - (L_m^2/L_s * L_r)$$

Here $X_{e(k)}$ is extended state vector, $U_{(k)}$ is control input vector, f is the non-linear state and input function, h is the output function, $W_{(k)}$ is process noise, $V_{(k)}$ is measurement noise, A_d is the extended system matrix, B_d is control input matrix, C_d is the measurement matrix and $Y_{(k)}$ is the output measurement vector. The matrix form of IM state space model is formed using (8) - (11) is used in EKF algorithm, which involves following steps.

1. Initialize the states $X_{(0/0)}$, error covariance matrix $P_{(0/0)}$, and covariance matrices Q and R, where $Q = E\{W_{(k)}.W_{(k)}^T\}$ and $R = E\{V_{(k)}.V_{(k)}^T\}$.
2. Prediction of state vector $X_{(k+1)\backslash k}$ from motor state equations at time 'k'.

$$X_{(k+1)\backslash k} = A_d X_{k\backslash k} + B_d U_k \quad (12)$$

3. Prediction of error covariance matrix $P_{(k+1)\backslash k}$ before new measurements are made at time 'k'.

$$P_{(k+1)\backslash k} = F_k P_{k\backslash k} F_k^T + Q \quad (13)$$

$$P_{(k+1)\backslash k} = E\{e_{(k+1)}.e_{(k+1)}^T\} \quad (14)$$

$$e_{(k+1)} = X_{(k+1)} - X_{k+1\backslash k} \quad (15)$$

$$F_k = \left.\frac{\partial f(X_{e(k)}, U_{(k)})}{\partial X_{e(k)}}\right|_{X_{k\backslash k}} \quad (16)$$

4. Calculate Kalman gain

$$K_{(k+1)} = P_{(k+1)\backslash k} H_k^T + \left[H_k P_{(k+1)\backslash k} H_k^T + R\right]^{-1} \quad (17)$$

$$H_k = \left.\frac{\partial h(X_{e(k)})}{\partial X_{e(k)}}\right|_{X_{k\backslash k}} \quad (18)$$

5. Correction and measurement updating state

$$X_{(k+1)\backslash(k+1)} = X_{(k+1)\backslash k} + K_{(k+1)} * \left[Y_{(k+1)} - C_d X_{(k+1/k)}\right] \quad (19)$$

$$P_{(k+1)\backslash(k+1)} = [I - K_{(k+1)} H_k] P_{(k+1)\backslash k} \quad (20)$$

Here, F_k represents the linearised non-linear model of IM called gradient matrix; $X_{(k+1)\backslash k}$ and $X_{(k+1)\backslash(k+1)}$ represent the priori and the posteriori state estimations respectively; $P_{(k+1)\backslash k}$ and $P_{(k+1)\backslash(k+1)}$ represent the priori and the posteriori error covariance matrix; H_k and I represent the linearised non-linear measurement matrix and identity matrix, respectively.

Once the state variables are estimated using EKF algorithm, magnitude and instantaneous position of rotor field can be calculated using (21) and (22).

$$\lambda_r = \sqrt{\lambda_{r\alpha}^2 + \lambda_{r\beta}^2} \quad (21)$$

$$\theta_e = \tan^{-1}\left(\lambda_{r\beta}/\lambda_{r\alpha}\right) \quad (22)$$

Speed of rotor field can be determined using estimated rotor speed and rotor flux which is given by (23).

$$\omega_e = \omega_r + \frac{L_m}{T_r} * \frac{i_{qs}}{\lambda_r} \quad (23)$$

IV. Simulation Results

RFOC-based closed-loop IM drive system with fault-tolerant control and state estimation are modelled and evaluated in MATLAB/SIMULINK platform in accordance with Fig. 1 and Fig. 4. Table II shows the rating and parameters of the drive used for simulation study. Voltage and frequency control in the inverter is achieved through sine PWM modulation with a switching frequency of 5 kHz. Initial values of all the estimated state vectors in the EKF-based estimation algorithm are taken as zero and trial-and-error method is used to determine the covariance matrices Q and R.

$Q = \text{diag}\{10^{-6}\ 10^{-6}\ 10^{-12}\ 10^{-12}\ 10^{-5}\}$

$R = \text{diag}\{10^{-5}\ 10^{-5}\}$

with the sampling time of $T_s = 10\mu s$

The performance of fault-tolerant control is tested for one open-phase fault condition with a speed reference of 1200 rpm and with rated rotor flux of 0.88 Wb. At $t = 1.5$ s, load torque is gradually increased from no-load to full load of 17 Nm within 0.5 sec, and at a reference speed of 1200 rpm. At $t = 3$ s, open-circuit fault is made in upper switch of phase-A i.e., S_1. Phase-A is isolated at t=3.1 sec. At $t = 3.2$ s, fault-tolerant control is activated.

Torque response of the drive is shown in Fig. 5. It can be observed from the figure that the torque ripple is slightly increased after applying the FTC algorithm due to non-zero values of harmonic current references generated by the fault-tolerant algorithm. Current references can be modified to minimise the torque ripple however, it is out of scope of this paper. From the speed response of the drive shown in Fig. 6, it is clear that the drive is able to track the reference speed during the continuous change in the load implies the accurate and fast dynamic response of the RFOC-based drive. The estimated speed tracks the actual speed very closely during both pre-fault and post-fault operations with minimum estimation error. The maximum estimation error is found to be 10 rpm under no load condition of the motor. The FTC algorithm is activated at $t = 3.2$ s and the drive is able to regain the pre-fault operating point within 0.5 sec, which indicates the effectiveness of RFOC-based FTC. Estimated flux follows the actual flux during both during both pre-fault and post-fault operations with minimum estimation error of 0.018 Wb which is evident in Fig. 7.

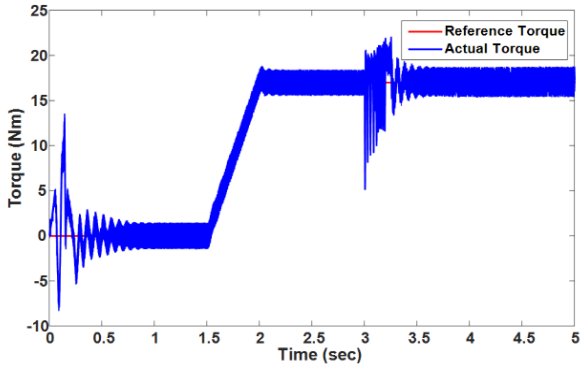

Fig. 5. Torque response of the drive

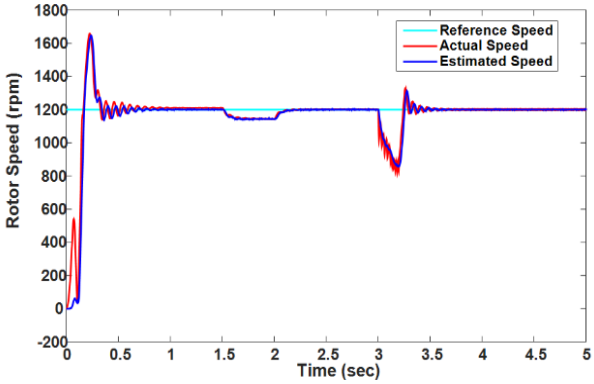

Fig. 6. Actual and estimated speed response of the drive for change in load

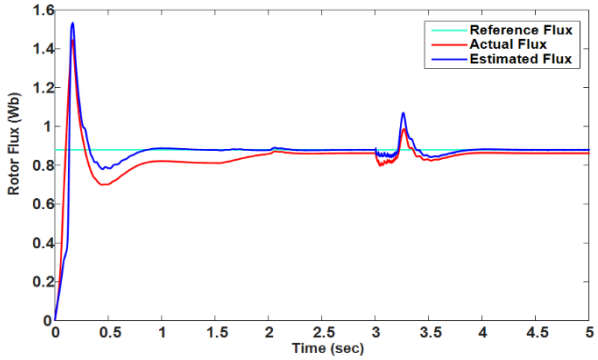

Fig. 7. Actual and estimated rotor flux

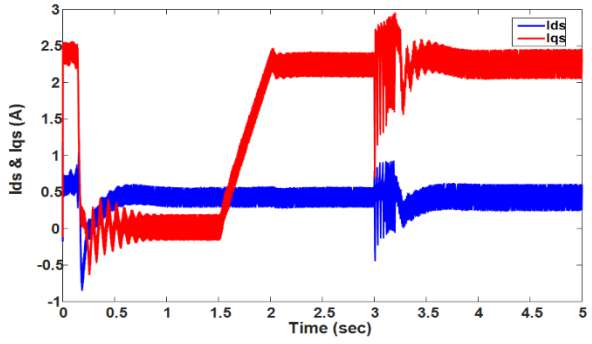

Fig. 8. Flux component (I_{ds}) and torque component (I_{qs}) of stator current

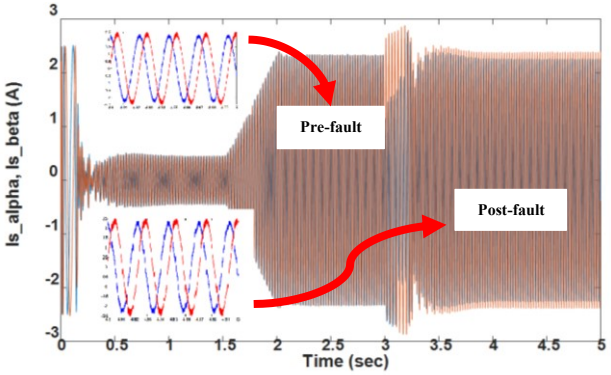

Fig. 9. Orthogonal stator current components $i_{s\alpha}$ and $i_{s\beta}$ in stationary reference frame

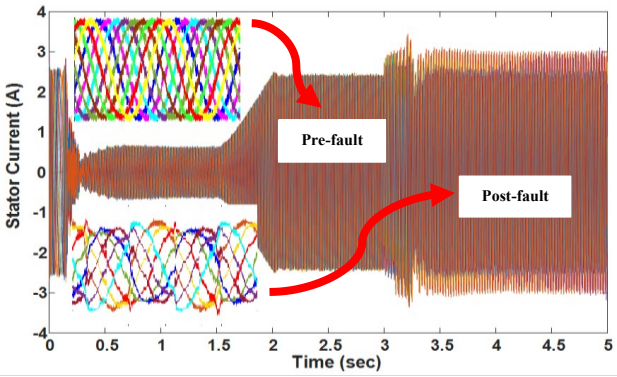

Fig. 10. Stator current variation during pre-fault and post-fault operations

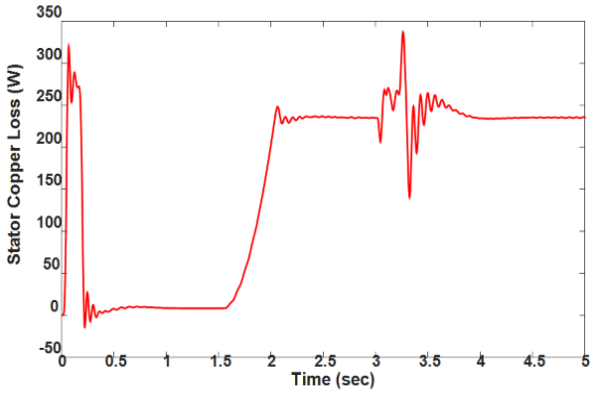

Fig. 11. Stator copper loss in induction motor during prefault and post-fault operations

The torque component and flux component of stator current in rotor field-oriented reference frame and stationary reference frame are shown in Fig. 8 and Fig. 9, which indicate the accurate orientation of rotor flux reference frame which is determined using EKF algorithm. The stator current variation during change in load and faulty conditions are shown in Fig.10. The current distribution during pre-fault and post-fault conditions are also indicated in the figure. The phase current magnitudes during post-fault are found to be unequal because the FTC is trying to maintain the operating condition and stator copper loss same as

in pre-fault stage. The stator copper loss in the machine during full load is shown in Fig. 11. The stator copper loss is found to be same in both pre-fault and post-fault operations of the drive, which indicates the effectiveness of the proposed fault-tolerant control. The above discussed drive performance is quantified in Table I.

TABLE I. PERFORMANCE ANALYSIS OF FTC

Quantity	Pre-fault value	Post-fault value
Speed (rpm)	1200	1200
Torque (Nm)	17	17
Torque Ripple (%)	4.7	7.6 41.17 without FTC
Stator Copper Loss (W)	235	235.4
Rotor Copper Loss (W)	180	183
Maximum & Minimum phase current (amps) (rms)	1.69 & 1.69	2.12 & 1.55

TABLE II. PARAMETERS USED FOR SIMULATION

Induction motor power rating	3 HP
Rated speed (N)	1426 rpm
Rated frequency of motor (f)	50 Hz
Rated phase current of motor (A)	2.1 A
Rated phase voltage of motor (V)	220 V
Stator and rotor self-inductances (L_S, L_r)	0.46 H
Stator and rotor resistances (R_S, R_r)	10 Ω, 6.3 Ω
Magnetizing inductance (L_m)	0.42 H
Rated DC-link voltage (V_{dc})	615 V
Inverter switching frequency (f_s)	5 kHz
Moment of inertia of motor and load (J)	0.03 kg-m^2
Viscous Friction coefficient (b)	0.003 Nm-sec

V. CONCLUSION

A fault-tolerant control for nine-phase induction motor drive with open circuit fault in inverter legs is presented in this paper. The extended Kalman filter is used for the estimation of rotor speed and rotor field orientation, makes the system more reliable and less sensitive to motor parameter variations and measurement noises. It can be inferred from the simulation results that the RFOC-based fault-tolerant control is able to track the speed and flux references accurately during wide change in load torque in the machine. The IM drive states are estimated accurately with minimum estimation error during both pre-fault and post-fault operating conditions. FTC is able to limit the torque ripple during one phase O.C. fault while maintaining the rated motor copper losses. The comparison, in terms of stator and rotor copper losses, torque ripple, and max/min of phase currents is carried out by considering the first four spatial harmonics of the air-gap MMF.

REFERENCES

[1] J. O. Estima and A. J. M. Cardoso, "A new approach for real-time multiple open-circuit fault diagnosis in voltage-source inverters," IEEE Trans. Ind. Appl., vol. 47, no. 6, pp. 2487–2494, Nov-Dec. 2011.

[2] Z. Liu, Z. Zheng, and Y. Li, "Enhancing fault-tolerant ability of a nine-phase induction motor drive system using fuzzy logic current controllers," IEEE Trans. Energy Convers., vol. 32, no. 2, pp. 759–769, 2017.

[3] T. A. Lipo, "Disturbance-free operation of a multiphase current-regulated motor drive with an opened phase," IEEE Trans. Ind. Appl., vol. 30, no. 5, pp. 1267–1274, 1994.

[4] E. Levi, R. Bojoi, F. Profumo, H.A. Toliyat and S. Williamson "Multiphase induction motor drives- A technology status review," IET Electr. Power Appl., vol. 1, no. 5, pp. 643–656, 2007.

[5] E. Levi, "Multiphase electric machines for variable-speed applications," IEEE Trans. Ind. Electron., vol. 55, no. 5, pp. 1893–1909, 2008.

[6] G. Tang, W. Kong, and T. Zhang, "Optimized non-sinusoidal SVPWM method for high power multiphase induction motor drives," J. Power Electron., vol. 20, no. 4, pp. 938–947, 2020.

[7] Z. Wang, X. Wang, Y. Wang, J. Chen, and M. Cheng, "Fault tolerant control of multiphase multilevel motor drives - Technical review," Chinese J. Electr. Eng., vol. 3, no. 2, pp. 76–86, 2017.

[8] T. S. de Souza, R. R. Bastos and B. J. C. Filho, "Fault analysis in an inverter-fed nine-phase induction machine," 2017 IEEE Energy Conversion Congress and Exposition (ECCE), 2017, pp. 371-378.

[9] T. S. de Souza, R. R. Bastos and B. J. Cardoso Filho, "Fault-tolerant operation of a nine-phase induction machine with open phases," 2017 IEEE Industry Applications Society Annual Meeting, 2017, pp. 1-9.

[10] H. M. Ryu, J. H. Kim, and S. K. Sul, "Analysis of multiphase space vector pulse-width modulation based on multiple d-q spaces concept," IEEE Trans. Power Electron., vol. 20, no. 6, pp. 1364–1371, Nov. 2005.

[11] Nair, N. S., & Jagadanand,. "A new inverter fault detection scheme for nine-phase induction motor drive system," PESGRE 2022 - IEEE International Conference on Power Electronics, Smart Grid, and Renewable Energy," pp. 1–6, 2022.

[12] J. W. Kelly, E. G. Strangas, and J. M. Miller, "Multiphase space vector pulse width modulation," IEEE Trans. Energy Convers., vol. 18, no. 2, pp. 259–264, June 2003.

[13] Texas Instruments, Europe, T. I. (1997). "Sensorless control with Kalman filter on TMS320 Fixed-Point DSP," Literature Number: BPRA057 1997.

[14] El-Barbary, Z. M. S., "Low-cost fault tolerant based speed sensorless vector control of induction motor drive system.," Journal of Electrical Systems, 9(3), 315–328. 2013.

[15] Barut, M., Bogosyan, S., & Gokasan, M. "Speed-sensorless estimation for induction motors sing extended Kalman filters," IEEE Transactions on Ind. Electron., 54(1), 272–280, 2007.

[16] Modern Power Electronics and AC Drives, Bimal K. Bose, Prentice Hall.

[17] Yildiz, R., Barut, M., & Demir, R., "Extended Kalman filter based estimations for improving speed-sensored control performance of induction motors," IET Electric Power Appl., 14(12), pp. 2471–2479. Sep. 2020.